

1 **An adaptive auto-reduction solver for speeding up integration of chemical**
2 **kinetics in atmospheric chemistry models: implementation and evaluation in**
3 **the Kinetic Pre-Processor (KPP) version 3.0.0**

4 **Haipeng Lin¹, Michael S. Long¹, Rolf Sander², Adrian Sandu³, Robert M. Yantosca¹, Lucas**
5 **A. Estrada¹, Lu Shen⁴, Daniel J. Jacob¹**

6 ¹John A. Paulson School of Engineering and Applied Sciences, Harvard University, Cambridge, MA 02138,
7 USA

8 ²Air Chemistry Department, Max Planck Institute for Chemistry, Mainz 55020, Germany

9 ³Department of Computer Science, Virginia Polytechnic Institute and State University, Blacksburg, VA
10 24060, USA

11 ⁴Department of Atmospheric and Oceanic Sciences, School of Physics, Peking University, Beijing 100871,
12 China

13 Corresponding author: Haipeng Lin (hplin@seas.harvard.edu)

14
15 **Key Points:**

- 16 ● An updated version 3.0.0 of the Kinetic Pre-Processor (KPP) integrator of chemical kinetics for
17 atmospheric models has been developed.
- 18 ● KPP 3.0.0 features an adaptive solver option for reducing chemical mechanisms locally and on the
19 fly where full complexity is not needed.
- 20 ● The adaptive solver implemented in the global GEOS-Chem model shows a 32% speedup with
21 errors less than 1% for key tropospheric species.

22 **Abstract**

23 Kinetic integration of large and stiff chemical mechanisms is a computational bottleneck in models of
24 atmospheric chemistry. It requires implicit solution of the coupled system of kinetic differential equations
25 with time-consuming construction and inversion of the Jacobian matrix. We present here a new version of
26 the Kinetic Pre-Processor (KPP 3.0.0) for fast integration of chemical kinetics featuring a range of
27 improvements over previous versions in performance, diagnostics, versatility, and community openness.
28 KPP 3.0.0 includes a new adaptive auto-reduction solver to decrease the size of any mechanism locally and
29 on the fly under conditions where full complexity is not needed, by partitioning species as “fast” or “slow”
30 based on their local production and loss rates. Previous implementations of this adaptive solver suffered
31 from excessive overhead in the repeated construction of the local Jacobian matrix or were hard-wired to
32 specific mechanisms. Here we retain the general applicability of the method to any mechanism and avoid
33 overhead by using pre-computed Jacobian matrix terms for the full mechanism and cropping the matrix
34 locally to remove the slow species with no change in memory allocation. We apply this adaptive solver
35 within KPP 3.0.0 to the GEOS-Chem global 3-D model of atmospheric chemistry and demonstrate a 32%
36 reduction in solver time while maintaining a mean error lower than 1% for key species in the troposphere.

37

38 **Plain Language Summary**

39 Calculating chemical evolution in global atmospheric chemistry models is computationally expensive
40 because the chemical mechanisms typically include hundreds of species to account for all conditions from
41 urban to remote. However, the full chemical complexity is not needed under most conditions. Here we have
42 developed an adaptive auto-reduction chemical solver that reduces any mechanism on the fly depending on
43 local conditions and without significant computational overhead. We apply this adaptive solver as an option
44 in a new version 3.0.0 of the Kinetic Pre-Processor (KPP) chemical solver software package that also
45 includes a number of updates relative to previous versions. The adaptive solver achieves a 32% reduction
46 in solver time in a global model simulation while incurring less than 1% average errors for key species.

47 **1 Introduction**

48 Modeling atmospheric chemistry is a grand computational challenge. Current global 3-D models of oxidant-
49 aerosol chemistry use chemical mechanisms that may involve hundreds of coupled chemical species with
50 lifetimes ranging from less than a second to many years. Chemical evolution in such a mechanism is
51 computed by solving a large, stiff system of coupled non-linear ordinary differential equations (ODEs)
52 expressing the chemical kinetics of individual species. Implicit solvers are required to accommodate the
53 coexistence of short and long time constants but are computationally expensive because of the need for
54 repeated construction and inversion of the Jacobian matrix (Brasseur & Jacob, 2017). Chemical integration
55 often dominates the overall computational cost of global 3-D atmospheric chemistry model simulations,
56 even in massively parallel environments or using graphics processing units (GPUs) (Alvanos &
57 Christoudias, 2017; Eastham et al., 2018; Zhuang et al., 2020; Dawson et al., 2022).

58
59 Considerable research has gone into devising algorithms to speed up chemistry solvers. A common strategy
60 is to split the mechanism species by time scales in order to decrease the stiffness of the system (Young &
61 Boris, 1977; Gong & Cho, 1993; Djouad & Sportisse, 2002), but this tends to be mechanism-specific and
62 is difficult to apply in global models because of the wide range of conditions that may be experienced.
63 Wholesale reduction of the mechanism, such as in the Super-Fast mechanism used in some climate models
64 (Brown-Steiner et al., 2018), may lead to large errors (Kelp et al., 2022) and incorrect chemical responses
65 to perturbations. Machine learning methods can in principle speed up chemical integration by orders of
66 magnitude but have met with little success because of the large dimensionality of the problem resulting in
67 error growth, in addition to requiring re-training and re-evaluation after even minor updates to the chemical
68 mechanism (Keller & Evans, 2019; Kelp et al., 2020, 2022).

69
70 A promising approach for global models is to recognize that the full complexity of the mechanism is not
71 needed everywhere. For example, reactions involving volatile organic compounds (VOCs) and their short-
72 lived products typically account for much of the complexity but may be unimportant outside of continental
73 boundary layers where the VOCs are emitted. Jacobson (1995) thus applied separate mechanisms in a global
74 model for the urban boundary layer, the global troposphere, and the stratosphere. However, fixed
75 geographical separation between domains can result in errors and inefficiencies by not accounting for the
76 interactions at chemical boundaries between domains (Rastigejev et al., 2007) and not allowing for a
77 continuum of chemical regimes from source regions to the remote atmosphere. Santillana et al. (2010)
78 developed an adaptive mechanism reduction method in which the size of the mechanism is adjusted at each
79 grid cell and time step, classifying species as fast (coupled) or slow (uncoupled) on the basis of their total

80 production and loss rates. However, the overhead involved in local definition of the reduced mechanism
81 offset the computational gains. Sander et al. (2019) and Shen et al. (2020, 2022) improved the method by
82 pre-compiling a limited ensemble of chemical sub-mechanisms and selecting the most appropriate sub-
83 mechanism for use based on local conditions at each timestep, thus avoiding the overhead. Shen et al.
84 achieved a 30%-50% reduction in computational cost compared to the full parent mechanism in a global
85 simulation of the troposphere and stratosphere, but the selection of sub-mechanisms had to be customized
86 to the parent mechanism.

87
88 Here we develop a mechanism-agnostic, ready-to-use method for adaptive auto-reduction of any chemical
89 mechanism and implement it as an option in a new version 3.0.0 of the Kinetic PreProcessor (KPP).
90 Originally developed by Damian et al. (2002) and Sandu and Sander (2006), KPP is a software tool that
91 automatically generates code to efficiently integrate chemical mechanisms. KPP takes in a set of human-
92 readable input files describing the mechanism and generates Fortran 90, C, or MATLAB code to solve the
93 corresponding system of ODEs using any of a suite of integration methods. KPP is used in many
94 atmospheric chemistry models including MECCA within MESSy (Sander et al., 2019; Jöckel et al., 2010),
95 WRF-Chem (Grell et al., 2005; Fast et al., 2006), the forward and adjoint GEOS-Chem models (Henze et
96 al., 2007), and the adjoint for the CMAQ model (Hakami et al., 2007; Zhao et al., 2020). Our new version
97 KPP 3.0.0 incorporates several performance and diagnostic updates over the previous version KPP 2.1
98 (Sandu & Sander, 2006) in addition to the adaptive solver option.

99 **2 Adaptive solver for chemical kinetics**

100 Atmospheric chemistry models alternate chemical integration and transport calculations through operator
101 splitting (Brasseur & Jacob, 2017). The chemistry solver is called for a time interval of length Δt , referred
102 to as the external time step, and returns a vector of updated concentrations \mathbf{C} at the end of that time step to
103 be operated on by transport. The kinetic integration of the mechanism by the chemistry solver is done over
104 internal time steps $h \leq \Delta t$ to reach the desired accuracy.

105
106 The chemistry solver integrates a system of N coupled nonlinear first-order ODEs of the form

$$107 \quad \frac{dC_i}{dt} = P_i(\mathbf{C}) - L_i(\mathbf{C}) \quad (i = 1, 2, \dots, N) \quad (1)$$

108 where N is the number of coupled species in the mechanism, \mathbf{C} is the vector of species concentrations of
109 dimension N , and $P_i(\mathbf{C})$ and $L_i(\mathbf{C})$ are the production and loss rates of species i that depend on the
110 concentrations of other species in the mechanism through the reaction rate expressions.

111

112 The external time step in a global model is typically $\sim 10^3$ s, but many species in the mechanism have
113 lifetimes ~ 1 s or shorter. An explicit solver would require internal time steps shorter than the lifetime of the
114 shortest-lived species in order to achieve stability, but this is not computationally practical. An implicit
115 solver is required. The simplest such solver is the first-order backward Euler method, which approximates
116 the solution to (1) over the internal time step h with

$$117 \quad \mathbf{C}(t+h) = \mathbf{C}(t) + \mathbf{s}(\mathbf{C}(t+h))h \quad (2)$$

118 where we define the net source term $\mathbf{s} = \mathbf{P} - \mathbf{L}$ as a vector of functions ($P_i - L_i$). Solving (2) for the
119 unknown quantity $\mathbf{C}(t+h)$ using the Newton-Raphson method requires the repeated construction and
120 inversion of the $N \times N$ Jacobian matrix \mathbf{J} :

$$121 \quad \mathbf{J} = \frac{\partial \mathbf{s}}{\partial \mathbf{C}} \quad (3)$$

122 The construction and inversion of this Jacobian matrix is computationally expensive. Higher-order solvers
123 generally used in atmospheric chemistry models, such as Rosenbrock (Rosenbrock, 1963; Hairer & Wanner,
124 1991; Sandu et al., 1997) or Gear (Jacobson & Turco, 1994), similarly require the repeated construction
125 and inversion of the Jacobian over internal time steps. The Jacobian is typically $\sim 90\%$ sparse allowing for
126 efficient sparse-matrix inversion methods (Sandu et al., 1997), so that the overall cost of construction and
127 inverting the Jacobian scales as $\sim N$ rather than a higher power.

128
129 A way to reduce the dimensionality N of the problem is to split the mechanism into “fast” species for which
130 the coupled implicit solution is necessary and “slow” species that may be solved independently over the
131 external time step using a fast explicit method. Young and Boris (1977) and Gong and Cho (2003) separate
132 species into fast and slow based on their lifetimes compared with the integration time step. However, the
133 separation results in non-conservation of mass because the reaction rates are not computed consistently.
134 This may not be of consequence in a regional model (as used in those applications) where the domain is
135 ventilated by the boundary conditions, so that errors do not accumulate, but it is more problematic in a
136 global model. Santillana et al. (2010) separated instead “fast” and “slow” species on the basis of their
137 production and loss rates, with the slow species having sufficiently low rates that their non-conservation of
138 mass would be inconsequential. This is more relevant for global models where concentrations and rates of
139 short-lived VOCs become very small and they have negligible influence on other species outside of their
140 source regions. Shen et al. (2020, 2022) used the same approach to partition species between fast and slow.

141
142 Here we also follow the partitioning method of Santillana et al. (2010). At the beginning of each external
143 time step we calculate \mathbf{P} and \mathbf{L} and classify species i as fast if $\max(P_i, L_i) > \delta$ and as slow otherwise,
144 where δ is a user-selected partitioning threshold. Fast species are assigned to the coupled implicit solver as

145 a subset (sub-mechanism) of the full mechanism, while the evolution of slow species over the external time
146 step beginning at t_0 is calculated using an explicit first-order approximation with first-order loss rate
147 constant $k_i(t_0) = L_i(t_0)/C_i(t_0)$:

$$148 \quad C_i(t_0 + \Delta t) = \frac{P_i(t_0)}{k_i(t_0)} + \left(C_i(t_0) - \frac{P_i(t_0)}{k_i(t_0)} \right) e^{-k_i(t_0)\Delta t} \quad (4)$$

149 In the Santillana et al. (2010) implementation, the Jacobian had to be reconstructed locally at every external
150 time step for the identified subset of fast species and that incurred large overhead, canceling the benefit of
151 the method. Here we avoid the overhead by taking advantage of the pre-computed Jacobian matrix terms
152 for the full mechanism in the KPP solver to simply remove rows and columns corresponding to the slow
153 species. This is explained in Section 3.2 and is the key new development to make the method
154 computationally practical.

155
156 The partitioning threshold δ is set prior to integration and is tuned to balance performance and accuracy.
157 Previous work (Santillana et al., 2010; Shen et al, 2020, 2022) considered that in a typical tropospheric
158 chemistry mechanism, much of the coupling is associated directly or indirectly with cycling of the hydroxyl
159 radical (OH). OH has a daytime concentration of $\sim 10^6$ molecules cm^{-3} and a lifetime ~ 1 s, so its production
160 and loss rates are $\sim 10^6$ molecules $\text{cm}^{-3} \text{ s}^{-1}$. A species with production and loss rates that are several orders
161 of magnitude smaller would not be expected to contribute significantly to the coupling. They found
162 $\delta \sim 10^2 - 10^3$ molecules $\text{cm}^{-3} \text{ s}^{-1}$ to be adequate after testing for performance and accuracy.

163
164 Here we include the option to dynamically define δ instead of specifying a uniform value over the domain,
165 to account for rates varying with local conditions. This is done by identifying a target species which is
166 considered central to the mechanism and scaling its production and loss rates to define a local partitioning
167 threshold:

$$168 \quad \delta = \alpha_{\text{target}} \max(P_{\text{target}}, L_{\text{target}}) \quad (5)$$

169 where P_{target} and L_{target} are the local production and loss rates of the target species, and $\alpha_{\text{target}} \ll 1$ is
170 a user-selected coefficient that depends on the target species but is otherwise fixed for the model domain.
171 For example, a model may use OH as target species for daytime, and NO_2 or the nitrate radical (NO_3) for
172 nighttime. When using OH as a target species and with $\max(P_{\text{OH}}, L_{\text{OH}}) \sim 10^6$ molecules $\text{cm}^{-3} \text{ s}^{-1}$, a value
173 $\alpha_{\text{OH}} \sim 10^{-4} - 10^{-3}$ would correspond to the criteria for δ used by Santillana et al. (2010). But
174 $\max(P_{\text{OH}}, L_{\text{OH}})$ can in fact vary over orders of magnitude depending on pressure, UV flux, and other factors,
175 and our local specification of δ accounts for this variability. We find that this specification of dynamic
176 threshold improves accuracy with no significant overhead since P_{target} and L_{target} are computed at the
177 beginning of each external time step in any case.

178
179 We also include two new options in the algorithm. First is to force individual species to remain in the
180 coupled implicit solver even if $\max(P_i, L_i) \ll \delta$. As we will see, this may be helpful for inorganic halogen
181 species that cycle between radical and non-radical forms across sunrise/sunset. Second is to include an
182 ‘append’ functionality in the algorithm so that a species initially diagnosed as slow at the beginning of the
183 external time step can be transferred into the coupled implicit solver if it becomes fast over the course of
184 the integration. This increases accuracy with minimum overhead.

185 **3 Kinetic Pre-Processor (KPP) version 3.0.0**

186 **3.1 KPP 3.0.0 overview**

187 KPP (Damian et al., 2002; Sandu & Sander, 2006) generates code for solving the chemical kinetics for a
188 given chemical mechanism defined by a list of species, reactions, and rate constants. It is designed for speed
189 by exploiting sparse matrix algebra and pre-computation of terms. We have made several improvements to
190 KPP relative to the previous version 2.1 (Sandu & Sander, 2006), including the adaptive solver option. We
191 present these improvements as KPP version 3.0.0, available for download from
192 <https://github.com/KineticPreProcessor/KPP/> (DOI: 10.5281/zenodo.7308373) with detailed
193 documentation at <https://kpp.readthedocs.io>. Existing features in the previous versions of KPP are
194 maintained in KPP version 3.0.0. Our new version has zero numerical differences compared to KPP version
195 2.1 when using the same configuration as verified using the “saprc2006.kpp” example.

196
197 KPP takes in as input one or more text files, with an example shown in Figure 1. The input is not necessarily
198 in one single file; it may be split into several files for readability. The files describe the chemical mechanism,
199 the choice of numerical solver (e.g., Rosenbrock), target language (i.e., Fortran 90, C, or MATLAB),
200 floating point type (single- or double-precision), production and loss diagnostics for selected chemical
201 families (optional), and whether to use the adaptive solver option (optional). Some inputs are not part of
202 the KPP code generation and are instead left for users to adjust at runtime, including convergence criteria
203 (absolute and relative tolerance), numerical order of the solver, and adaptive solver options, in order to
204 enable the user to experiment with different thresholds for performance and accuracy.

```

#INTEGRATOR   rosenbrock_autoreduce
#LANGUAGE     Fortran90
#MINVERSION   3.0.0
#AUTOREDUCE   on
#FAMILIES
POx : O3 + NO2 + HNO3;
LOx : O3 + NO2 + HNO3;

#DEFVAR
O3   = IGNORE;
NO   = IGNORE;
...

#EQUATIONS
O3 + hv = 2OH + O2 : PHOTOL(1);
NO + O3 = NO2 + O2 : ARR(1.8d-12, -1370.0);
CO + OH = CO2 + H2O : 2.4d-13;
H2O + NO = OH + NO2 : ARR(3.7d-12, 240.0);
NO2 + hv = NO + O3 : PHOTOL(2);
H2O + H2O = H2O2 + O2 : ARR(1.2d-13, 749.0);
H2O2 + hv = 2OH : PHOTOL(3);
CH4 + OH = CO + H2O : ARR(3.1d-12, -187.0);
...

```

KPP Options
Integrator, target language, and other code generation options

Production and Loss Families (Optional)

Definition of species
"IGNORE" if mass balance checks are not required
Otherwise specify stoichiometric composition

List of reactions
Reactants = Products : Rate constant
Fortran 90 expressions are supported in rate constants

205
206 **Figure 1. Example KPP input file.** The KPP input file includes options for code generation, adaptive auto-
207 reduction, diagnostics for production and loss rates of chemical families, and a list of species and reactions.
208 Reaction rate constants can be specified as expressions in the target language (in this case Fortran 90), here
209 showing calls to functions calculating photolysis and Arrhenius rate expressions.

210
211 Based on the specifications in the KPP input file(s), KPP creates files in the target language containing a
212 description of the system of ODEs (number of species, reactions, and a numbered list of species), code to
213 calculate the time derivatives, Jacobian matrix, and solution by back-substitution, along with a copy of the
214 numerical solver (such as Rosenbrock) and supporting routines for sparse linear algebra. This set of files
215 can be either run standalone as a box model or can be included in a 3-D model to update concentrations
216 locally over external time steps.

217
218 Auto-reduction of the mechanism with the adaptive solver described in Section 2 is an option in KPP 3.0.0
219 using the Fortran 90 language, enabled in the configuration file by #AUTOREDUCE on and specifying the
220 corresponding integrator (e.g., #INTEGRATOR rosenbrock_autoreduce). This sets up the
221 capability for the user to reduce the mechanism locally through specification of the partitioning threshold
222 δ between fast and slow species, listing any species for which this partitioning should not be applied. These
223 specifications are done at runtime for flexibility. Even when the auto-reduction solver is used, mechanism
224 auto-reduction can be disabled at runtime, defaulting to the behavior of the original integrator, to check for
225 accuracy. A test case box model for auto-reduction is included as part of KPP 3.0.0 documentation.

226

227 In addition to the option for adaptive mechanism auto-reduction, several additional features and
228 improvements were added to KPP 3.0.0 relative to the previous version 2.1 (Sandu & Sander, 2006). These
229 include:

230

231 **a. Redeployment of KPP source code, continuous integration, and documentation for community**
232 **development.** KPP 3.0.0 source code has been redeployed on GitHub for community development.
233 The GitHub repository incorporates continuous integration (CI) tests which automatically compile the
234 KPP source code to build and run combinations of sample chemistry mechanisms and integrators into
235 box models at every code revision. This helps to ensure that new features and updates added to KPP do
236 not break existing functionality and that numerical results for existing configurations are not affected.
237 The documentation has also been relocated to <https://kpp.readthedocs.io> where it is automatically built
238 with each code revision on GitHub.

239

240 **b. New diagnostics.** The following diagnostic features have been added to KPP 3.0.0:

241 • **Production and loss rates for chemical families.** KPP 3.0.0 allows for the definition of families of
242 chemical species for computing production and loss for that family, ignoring interconversion
243 reactions within the family. This is useful in models for example to keep track of odd oxygen (Bates
244 & Jacob, 2020) or nitrogen oxides. Families are defined in the #FAMILIES section of the KPP
245 input file.

246 • **Stoichiometric numbers.** The stoichiometric numbers of all reactions in the mechanism are now
247 available in the CalcStoichNum subroutine in the KPP-generated code. This feature is used to
248 calculate the importance of chemical species in a mechanism for the skeletal mechanism reduction
249 in Sander et al. (2019).

250 • **Individual reaction rates and time derivatives.** The reaction rates and their time derivatives are
251 now available as optional outputs from the KPP-generated code.

252

253 **c. Addition of new solvers.** Several solvers have been added as options for integrating chemical kinetics
254 including VODE (Brown et al., 1989), SDIRK (Hairer & Wanner, 1991), 3-stage Runge-Kutta, and
255 forward and backward Euler methods.

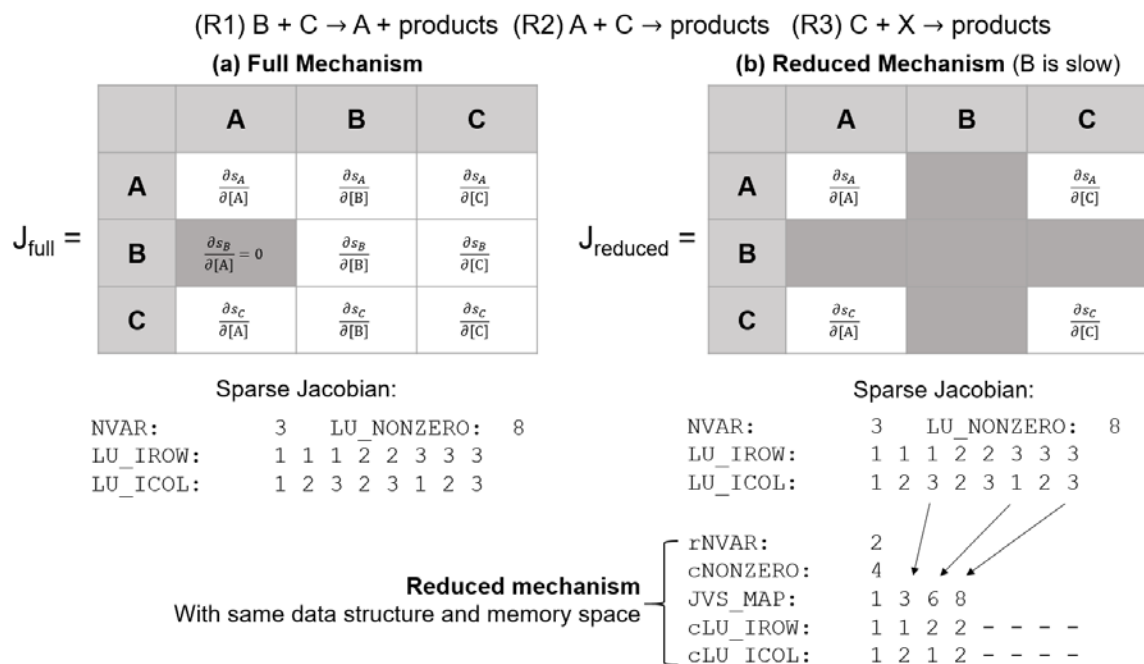
256

257 **d. Addition of new rate law functions.** Rate law functions for three-body reactions using the formulas
258 proposed by JPL (<https://jpldataeval.jpl.nasa.gov>) and IUPAC (<https://iupac.aeris-data.fr/>) have been
259 added to the built-in rate laws in KPP 3.0.0. Rate law functions are not limited to those built in KPP
260 and can be added by including extra source code files in the KPP input.

- 261
262 e. **Miscellaneous performance improvements in Fortran 90.** KPP 3.0.0 optimizes for Fortran 90
263 performance by applying several guidelines in coding, particularly in reaction rate calculations that are
264 computed repeatedly in loops:
- 265 • **Unifying number precision.** Previous inputs to KPP used both single- and double-precision
266 numbers. KPP input files and code now do not mix number precision to avoid conversion, which
267 loses precision and costs computational time.
 - 268 • **Switch to control update of reaction rate constants.** Previously, KPP called subroutines to update
269 reaction rate constants at every internal time step, but this is computationally expensive and may
270 not be needed in most model applications where the variables affecting rate constants are not
271 updated between internal time steps. An optional switch has been added so that rate constants are
272 updated only at the beginning of the external time step.
 - 273 • **Optimized rate law functions.** Rate law functions have been split to avoid computation of
274 unnecessary terms. For example, previously a single function with Arrhenius temperature
275 dependence was used for all reactions: $ARR_{abc}(A, B, C) = A * \exp(B/T) * (300/T)^C$. Many
276 reactions may have $B = 0$ or $C = 0$ but the expressions $300/T$ or $\exp(0)$ are still needlessly
277 computed. Separate rate functions such as $ARR_{ab}(A, B) = A * \exp(B/T)$ have been added,
278 leading to a 44% performance improvement of reaction rate computations in a full-chemistry
279 GEOS-Chem model run.
 - 280 • **Avoiding conditionals and optional arguments.** Conditional clauses such as IF, ELSE, and
281 SELECT CASE, and testing for optional arguments add significant computational cost if called
282 thousands of times. If a conditional clause or optional argument is present in a frequently called
283 subroutine, the subroutine is split into different functions for each case.
 - 284 • **Thread safety for generated code.** The code generated is now thread safe, so that calls for
285 updating rate constants and running the integrator can be placed in an OpenMP parallel loop for
286 parallelization.
 - 287 • **Improved expressions for vector and array functions.** Several functions for basic vector and
288 array operations originally used reference BLAS (Basic Linear Algebra Subprograms)
289 implementations. These have been replaced with Fortran 90 expressions to allow for compilers to
290 better optimize the code.
- 291
292 f. **Miscellaneous code improvements in KPP.** The C source code of KPP has been improved so that no
293 compiler warnings are generated. A more consistent memory allocation helps to avoid buffer overflow
294 problems. The KPP language is now parsed by `bison` instead of `yacc`.

305 **3.2 Adaptive solver implementation in KPP 3.0.0**

306 We implemented the adaptive solver as an option within KPP’s Fortran 90 version of the Rosenbrock solver
 307 using sparse matrix algebra. KPP is computationally efficient because the functions to compute the time
 308 derivatives for each species and the Jacobian matrix (expressed in terms of reaction rates and species
 309 concentrations), along with all sparse matrix algebra routines, are pre-generated and use fixed indices to
 310 access species vectors and matrices. This means that the problem size and memory space is fixed at compile
 311 time, avoiding expensive memory allocation operations. However, this also yields a fixed problem structure
 312 that is difficult to manipulate. One major source of overhead in locally defined sub-mechanisms as in
 313 Santillana et al. (2010) is associated with repeatedly re-allocating and de-allocating memory to
 314 accommodate changing problem sizes for each sub-mechanism (Shen et al., 2020). Our adaptive solver
 315 implementation in KPP 3.0.0 uses a mapping operation to project the full mechanism into sub-mechanisms,
 thus reusing the same memory space to avoid expensive resizing operations.



307
 308 **Figure 2. Mechanism auto-reduction in KPP.** Panel (a) shows the data structure of the sparse Jacobian
 309 data within KPP for a sample 3-species mechanism. If species B is diagnosed as slow, then the
 310 corresponding rows and columns of the Jacobian are no longer calculated (panel (b)), and the indices
 311 pointing to the sparse Jacobian data (LU_IROW, LU_ICOL) are adjusted to remove the slow species
 312 (cLU_IROW, cLU_ICOL) through a mapping array (JVS_MAP) while preserving the sparse matrix in
 313 row-compressed form. The result is a reduced mechanism with the same data structure as the original one,
 314 but with smaller dimensions.

316 Figure 2(a) shows the sparse Jacobian data as stored within KPP. In this example mechanism, there are 3
317 species (NVAR) and 8 non-zero entries in the Jacobian (LU_NONZERO) of the full mechanism. The row and
318 column indices of these 8 non-zero entries in Jacobian matrix are correspondingly specified in LU_IROW,
319 LU_ICOL in row-compressed form. At the beginning of every external time step, the production and loss
320 rates of each species are calculated and compared to the partitioning threshold to separate species into fast
321 and slow. Figure 2(b) shows an example where species B is slow. The entries in the Jacobian corresponding
322 to B no longer need to be computed, and a mapping operation is performed: JVS_MAP corresponds to the
323 non-zero Jacobian matrix entries still present in the sub-mechanism consisting of fast species. The smaller
324 sub-mechanism can now be described by 2 species (rNVAR) and 4 non-zero entries in the reduced Jacobian
325 (cNONZERO) with indices described by cLU_IROW and cLU_ICOL. The data structure of the smaller sub-
326 mechanism is identical to the full mechanism, and the same routines are used to solve it, without the need
327 to generate extra code, or resizing memory.

328
329 The mechanism auto-reduction is performed once at the beginning of every external time step. The set of
330 fast and slow species are established according to the runtime options for the partitioning threshold δ and
331 the list of species to be excluded from partitioning and kept in the fast subset under all conditions
332 (`keepSpcActive`). Based on the list of species in the fast set, the mapping (JVS_MAP) from the full
333 mechanism to the fast sub-mechanism is created. Because KPP generates hard-coded source code to
334 compute each term of the Jacobian matrix and back-substitution for computational efficiency, two logical
335 control vectors, `DO_JVS` and `DO_SLV`, are created to skip computation of terms corresponding to slow
336 species as these are no longer necessary.

337
338 The separation between fast and slow species is controlled by the initial conditions at the beginning of the
339 external time step, but an optional “append” function is added to account for an initially slow species
340 becoming fast over the course of the internal time steps. This function appends new species to the fast sub-
341 mechanism and adjusts the logical control vectors if these species are initially partitioned as slow but their
342 production or loss rate exceed the partitioning threshold over the course of the internal time stepping.
343 Diagnosing this has little overhead, because the production and loss rates of all species are already
344 computed at every internal time step.

345
346 We used a box model integration of the GEOS-Chem chemical mechanism (described below) to analyze
347 the overhead of the adaptive solver implemented within KPP. By forcing the adaptive solver routines to run
348 with a threshold of 0, we determined that the KPP overhead added by the auto-reduction is 10-16%. The
349 main source of overhead is the copying of data between the full and reduced sub-mechanism (Figure 2),

350 where the worst-case scenario is when all species are partitioned as fast and all species' data need to be
351 copied between the full to the "reduced" data structures. Profiling tests show that other steps such as the
352 partitioning of species between fast and slow, or the first-order approximation for slow species, contribute
353 negligible overhead.

354
355 We also used the box model to verify that our adaptive solver introduces minimal mass non-conservation
356 compared to the full solver. Integrating the box model over four sets of initial conditions from the GEOS-
357 Chem model over 10,000 time steps shows that the total masses of odd oxygen, reactive nitrogen, chlorine,
358 and bromine (defined in Table S1) are conserved within 0.30% in the standard configuration of the adaptive
359 solver as compared with the full mechanism solver. Figure S2 shows the geographical distribution of mass
360 non-conservation for these four families at a snapshot in time in a global GEOS-Chem model simulation,
361 again comparing the adaptive solver in its standard configuration to the full solver. Mass conservation is
362 within 0.01% for odd oxygen and reactive nitrogen and at worst within 0.2% for bromine.

363 **4 Adaptive mechanism auto-reduction in the GEOS-Chem model using KPP version 3.0.0**

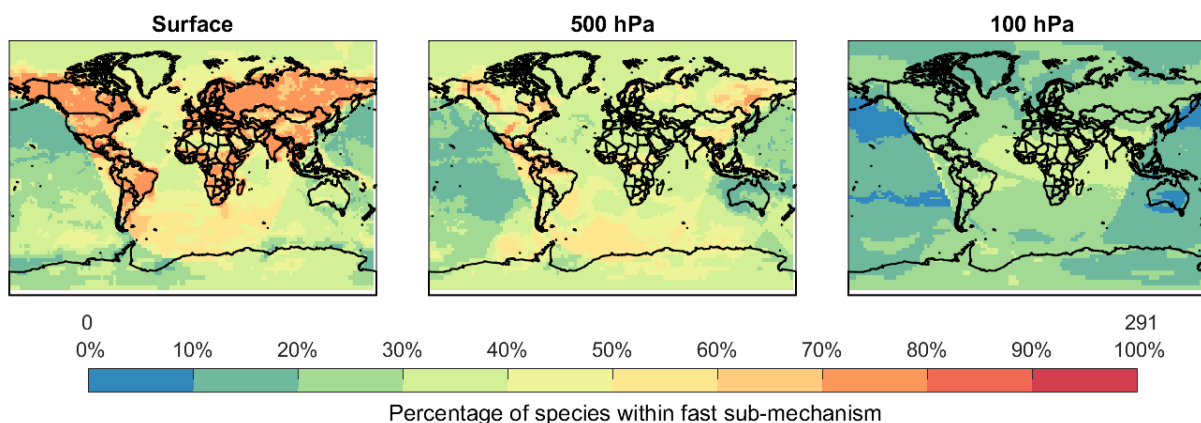
364 We demonstrate the adaptive solver capability in KPP version 3.0.0 with the GEOS-Chem global 3-D
365 atmospheric chemistry model version 13.4.0 (Bey et al., 2001; <https://doi.org/10.5281/zenodo.6511970>).
366 The chemical mechanism includes comprehensive oxidant-aerosol chemistry in the troposphere and the
367 stratosphere with 291 chemical species and 913 reactions. Recent updates to the mechanism include Cl-Br-
368 I tropospheric halogen chemistry (Wang et al., 2021), isoprene chemistry (Bates & Jacob, 2019), aromatic
369 chemistry (Bates et al., 2021), hydroxymethanesulfonate cloud chemistry (Moch et al., 2020), and NO_y
370 cloud and aerosol chemistry (Holmes et al., 2019). Heterogeneous sulfur chemistry that was previously
371 simulated with a separate module was brought into KPP in GEOS-Chem version 13.4.0 with the addition
372 of new rate functions.

373
374 GEOS-Chem has been structured to interact with the KPP-generated solver code through the FlexChem
375 interface which prepares data for the solver code, executes the code, and retrieves concentrations at the end
376 of the time step. FlexChem allows GEOS-Chem to use modules outside of KPP for computing reaction
377 rates, for example interfacing with Fast-JX for photolysis rates (Bian & Prather, 2002; Mao et al., 2010).
378 FlexChem also includes a derived type object, `State_Het`, which passes state variables from GEOS-
379 Chem model for calculating heterogeneous chemistry reaction rates including cloud liquid water content,
380 aerosol size distribution, pH, and alkalinity. This derived type object holds common intermediate quantities
381 necessary for heterogeneous reaction rate computations, such as aerosol area, avoiding repeated

382 computation and memory use. FlexChem also allows GEOS-Chem users to modify the chemical
383 mechanism input into KPP without modifying the GEOS-Chem source code.

384
385 We evaluate the accuracy and computational performance of the adaptive solver in KPP version 3.0.0 using
386 global GEOS-Chem simulations at $2^\circ \times 2.5^\circ$ resolution with 72 vertical levels extending up to 0.1 hPa. The
387 model is driven by the Modern-Era Retrospective analysis for Research and Applications, Version 2
388 (MERRA-2) meteorological fields from the NASA Global Modeling and Assimilation Office (GMAO).
389 The external time step for the chemistry solver is 20 minutes. All simulations are conducted on the same
390 single-node hardware with 24 Intel Cascade Lake physical cores (Intel(R) Xeon(TM) Platinum 8268 CPUs
391 with a base clock speed of 2.90GHz, no hyper-threading logical cores), 100 GB of RAM, and a high-
392 performance Lustre parallel file system. The model was compiled using Intel(R) Fortran Compiler (ifort)
393 version 2021.2.0.

394
395 We select as the standard configuration of the adaptive solver within the GEOS-Chem model a dynamically
396 defined threshold with OH as target species during daytime, and NO₂ during nighttime, with coefficients
397 $\alpha_{OH} = 5 \times 10^{-5}$ and $\alpha_{NO_2} = 1 \times 10^{-4}$. We find that using NO₃ as an alternative nighttime target species
398 results in higher accuracy but lower speed-up (Table S3). We do not force any species to remain in the
399 implicit KPP solver as fast and we do not use the append functionality. We find that we achieve a net 32%
400 reduction in integration time in this standard configuration.



401
402 **Figure 3. Percentage of GEOS-Chem species retained in the fast sub-mechanism when using the**
403 **adaptive solver.** The full GEOS-Chem mechanism has 291 species to describe tropospheric and
404 stratospheric oxidant-aerosol chemistry. Only a fraction of species is retained as fast in the KPP solver,
405 while the other species are solved individually using equation (4). Results are shown for a snapshot in time
406 on July 1, 2014, 12:00 UTC at different altitudes. The adaptive solver uses a dynamically defined threshold
407 (equation (5)) with target species OH in daytime ($\alpha_{OH} = 5 \times 10^{-5}$) and NO₂ at night ($\alpha_{NO_2} = 1 \times 10^{-4}$).

408 Figure 3 shows the percentage of species partitioned as fast (and hence retained in the KPP integration)
409 using the adaptive solver's standard configuration. Starting from the ensemble of 291 species in the GEOS-
410 Chem full mechanism, we find that over 60% are partitioned as fast in surface air over land, reflecting VOC
411 sources, whereas only 10-50% are partitioned as fast over the ocean. The fraction of retained species
412 decreases with altitude, and fewer than 40% are partitioned as fast in the stratosphere where VOC chemistry
413 is mainly limited to methane. Fewer species are partitioned as fast at night than in daytime. These results
414 are consistent with Shen et al. (2020).

415
416 We evaluate the accuracy of the adaptive solver (AS) relative to the full mechanism solver over the global
417 GEOS-Chem domain using the relative root mean squared (RRMS) error metric. For each species i , the
418 RRMS error is:

$$419 \quad RRMS_i = \sqrt{\frac{1}{N_i} \sum_{j=1}^{N_i} \left(\frac{C_{i,j,\text{full}} - C_{i,j,\text{AS}}}{C_{i,j,\text{full}}} \right)^2} \quad (6)$$

420 where $C_{i,j,\text{full}}$, $C_{i,j,\text{AS}}$ are the concentrations of species i in grid box j for simulations without and with the
421 adaptive solver. The RRMS is computed over the ensemble N_i of ordered grid boxes that account for 99%
422 of the total mass of species i in the boundary layer (surface to PBL height from MERRA2), free troposphere
423 (boundary layer height to tropopause), and stratosphere, respectively, and where $C_{i,j,\text{full}}$ is greater than 10
424 molecules cm^{-3} .

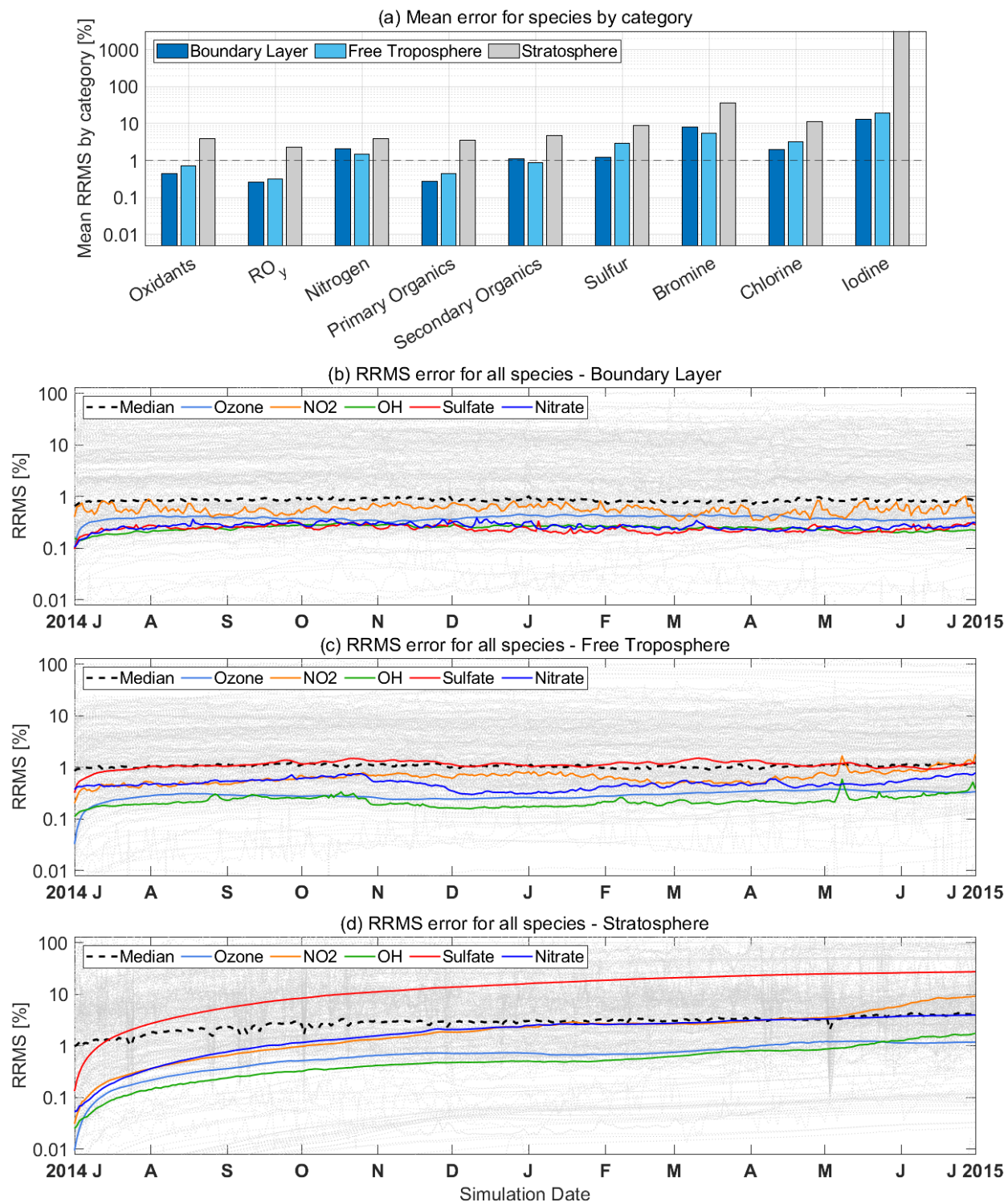
425
426 Figure 4(a) shows the mean errors at the end of a 1-year simulation for species in different chemical
427 categories (Table S4) and Figure 4(b)-(d) shows the time evolution of errors over the 1-year simulation for
428 all species in the standard configuration of the adaptive solver within the GEOS-Chem model, respectively.
429 The mean error for most categories is below 1% within the boundary layer and the free troposphere. There
430 is no error growth in the troposphere but there is some in the stratosphere. Figure 5 shows the geographical
431 distribution of relative errors (absolute errors shown in Figure S6) for ozone, OH, and NO_2 at the surface
432 and 500 hPa for the end of the 1-year simulation. Errors are generally lower than 1% except for OH at high
433 latitudes and NO_2 over the Southern Ocean, where errors are up to 3% for OH and 6~10% for NO_2 . Errors
434 over land for these species are minimal.

435
436 The largest errors in Figure 4 are found for inorganic halogen radicals and their reservoirs. Halogen radicals
437 cycle rapidly during the day but become locked in reservoirs at sunset, to be released again at sunrise (Wang
438 et al., 2021). Partitioning between fast and slow species at sunrise/sunset leads to large errors and mass
439 balance issues associated with the use of the first-order approximation (equation (4)). These problems were

440 previously identified by Shen et al. (2020, 2022). Long residence times in the stratosphere compound the
441 problem and drive slow error growth for other species. The impact is much less in the troposphere where
442 the inorganic halogens are removed by wet deposition.

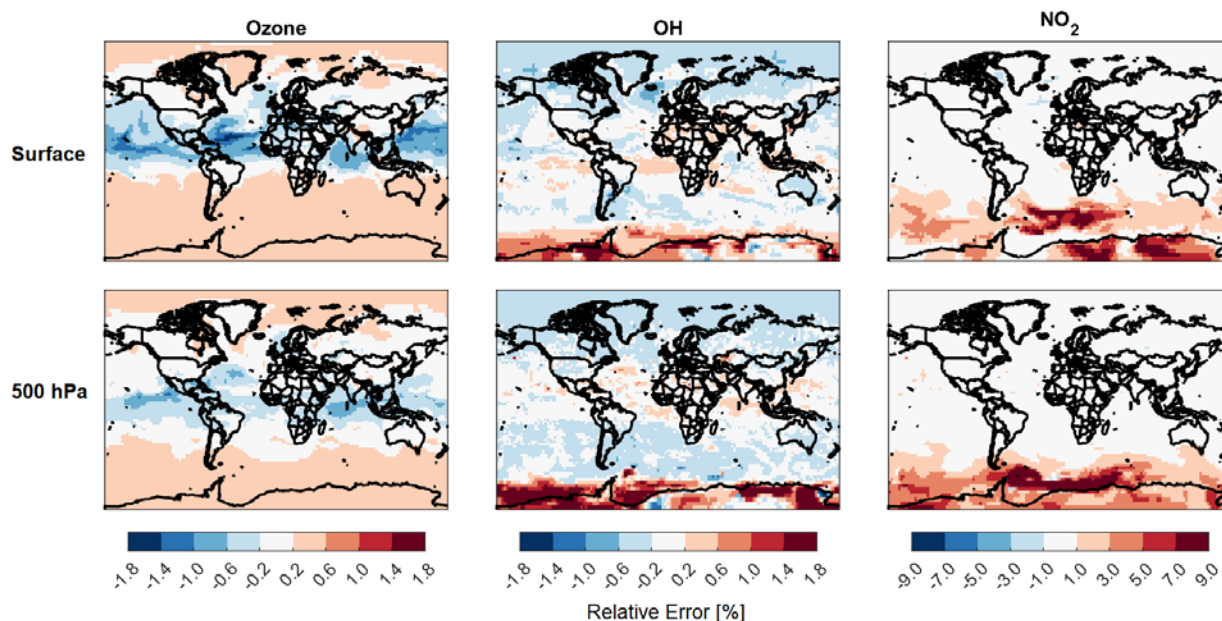
443
444 Our results in Figure 4 indicate that halogen species should be kept in the implicit solver as fast species if
445 the primary interest of the simulation is the stratosphere. Figure S5 shows the mean errors and time
446 evolution of errors over the 1-year simulation when halogen species are kept as fast in the adaptive solver.
447 In this configuration, the performance improvement of the adaptive mechanism is 23%, as compared to 32%
448 in the standard configuration. Keeping the halogen radicals and their reservoir species as fast prevents large
449 errors from developing in the stratosphere, in addition to avoiding error growth and spikes in errors as
450 shown in Figure 4(d). A similar problem though not of the same magnitude is found for hydrogen oxide
451 radicals controlling the concentration of OH in the stratosphere, and this causes high errors in stratospheric
452 sulfate exceeding 10% above 85 hPa. The list of species to be kept in the implicit solver in the GEOS-Chem
453 model can be configured in the *FlexChem* interface and passed to KPP 3.0.0 as a runtime option. An
454 alternative to customizing the list of species to be kept in the implicit solver is to disable the adaptive solver
455 in the stratosphere while retaining it in the troposphere. In this case, the performance improvement from
456 using the adaptive mechanism decreases from 32% to 20%. Such ad hoc adjustments to the fast/slow species
457 partitioning would be mechanism-specific and can be experimented with by users. We find in GEOS-Chem
458 that they are not needed for standard applications focusing on tropospheric chemistry.

459
460 We find in this application that the append functionality (allowing species to switch from slow to fast over
461 internal time steps) does not provide significant error reduction, in particular for the halogen species, and
462 degrades the performance improvement of the adaptive mechanism to 24% instead of 32%. We retain it as
463 an option in the adaptive solver code as it may be helpful for longer external time steps (here 20 minutes)
464 or other chemical mechanisms.



465
 466 **Figure 4. Accuracy of the adaptive solver in a 1-year GEOS-Chem simulation.** Panel (a) shows the
 467 mean RRMS errors for species in different categories at the end of the 1-year simulation starting on July 1,
 468 2014. The categories are as defined in the standard GEOS-Chem benchmarking output diagnostics (Table

469 S4). Panels (b)-(d) show the time evolution of RRMS errors for all species in the boundary layer, free
470 troposphere, and stratosphere, respectively, with colored lines for species of particular interest.
471 The adaptive solver uses a dynamically defined threshold (equation (5)) with target species OH in daytime
472 ($\alpha_{\text{OH}} = 5 \times 10^{-5}$) and NO_2 at night ($\alpha_{\text{NO}_2} = 1 \times 10^{-4}$), and does not force any species below that
473 threshold to remain as fast.



474
475 **Figure 5. Accuracy of the adaptive solver for ozone, OH, and NO_2 global distributions.** The Figure
476 shows the percent errors relative to the full solver for the daily mean concentrations on July 1, 2015, the
477 last day of the 1-year simulation, in surface air and at 500 hPa. The absolute error values corresponding to
478 this Figure are shown in Figure S6.

479
480 Our analysis of the performance and accuracy of the adaptive solver is based on 20-minute external time
481 steps for the chemistry solver in the GEOS-Chem standard $2^\circ \times 2.5^\circ$ configuration, but regional models with
482 finer grid resolution would use finer external time steps for operator splitting with transport (Philip et al.,
483 2016). We tested the sensitivity of our results to the size of the external time step within the GEOS-Chem
484 $2^\circ \times 2.5^\circ$ environment as shown in Table S3. We find that finer external time steps result in higher accuracy
485 but lower speed-up, which makes sense in terms of the overhead required at the beginning of each external
486 time step to define the sub-mechanism and cull the Jacobian, but also the opportunity to update the
487 separation between fast and slow species more frequently for better accuracy. Ultimately, this sensitivity to
488 external time-stepping will need to be tested by users in their own model environment (and their own
489 mechanism).

490 **5 Conclusions**

491 We presented an updated version of the Kinetic Pre-Processor (KPP 3.0.0) to integrate stiff chemical
492 mechanism kinetics typical of atmospheric chemistry models. KPP was originally designed for flexibility
493 and speed. KPP 3.0.0 features several improvements for performance, diagnostics, choice of solvers, and
494 code openness. It includes an adaptive solver capability for mechanism auto-reduction where and when the
495 full mechanism is not needed.

496
497 The adaptive solver performs auto-reduction of the chemical mechanism locally and on-the-fly at runtime,
498 by comparing the local production and loss rates of each species with a partitioning threshold (δ). Species
499 with production and loss rates higher than the threshold are considered fast and are solved as a coupled sub-
500 mechanism within KPP, while other species are considered slow and solved individually by an explicit
501 method. Previous application of this adaptive solver method suffered from large overhead due to the need
502 for local reconstruction of the reduced Jacobian matrix and the associated memory allocation and
503 deallocation. We solved this problem here by using pre-computed Jacobian terms for the full mechanism
504 with a mapping operation to crop rows and columns corresponding to the slow species without changing
505 the memory allocation.

506
507 KPP 3.0.0 features additional improvements for performance, diagnostics, versatility, and openness.
508 Improved performance includes more efficient calculation of reaction rates from the KPP rate functions
509 and thread safety for parallelization. New diagnostics include individual reaction rates, production and loss
510 rates for chemical families, and stoichiometric numbers. Improved versatility includes expanded choice of
511 chemical solvers. KPP 3.0 is now hosted on GitHub (<https://github.com/KineticPreProcessor/KPP>) to
512 enable community access, development, and testing.

513
514 We evaluated the adaptive solver implemented in KPP 3.0.0 by conducting a 1-year simulation with the
515 global 3-D GEOS-Chem atmospheric chemistry model including 291 species in the full mechanism for
516 oxidant-aerosol chemistry in the troposphere and stratosphere. Results show that a 32% performance
517 improvement in the solver can be achieved with a target error of 1% for key species in the troposphere.
518 Errors in the stratosphere can be larger, driven by halogen chemistry. Lower errors especially in halogen
519 species can be achieved by keeping these species within the fast sub-mechanism but this reduces the
520 performance improvement to 23% and is mainly beneficial in the stratosphere.

521

522 The release of KPP 3.0.0 introduces improvements in development infrastructure, diagnostics, and
523 performance, particularly in Fortran 90 applications. However, one of the strengths of the KPP software is
524 the capability to generate code for different programming languages. Development directions for future
525 versions include (1) adding support for modern languages such as Python and Julia; (2) refactoring of the
526 generated code to avoid global data structures for easier parallelization; (3) streamlining inputs and outputs
527 of all integrators for consistency; (4) supporting the adaptive solver option in other integrators and
528 programming languages; and (5) improving interaction and compatibility with the Master Chemical
529 Mechanism (<http://mcm.york.ac.uk>). These improvements will allow KPP to better serve the community
530 as a versatile tool for solving chemical kinetics within atmospheric chemistry models and other applications.

531 **Acknowledgements**

532 This work was supported by the US EPA Science to Achieve Results (STAR) Program, by the NASA
533 Modeling, Analysis, and Prediction (MAP) Program, and by the NASA Atmospheric Composition
534 Modeling and Analysis Program (ACMAP).

535

536 **Open Research**

537 *Data Availability Statement*

538 *Model Code Availability:* Source code for KPP 3.0.0 is available at

539 <https://github.com/KineticPreProcessor/KPP> (Sandu et al., 2022;

540 <https://doi.org/10.5281/zenodo.7308373>).

541 The adaptive solver box model is available at <https://github.com/KineticPreProcessor/KPP-AR->

542 [boxmodel/](https://github.com/KineticPreProcessor/KPP-AR-boxmodel/) (Long & Lin, 2022; <https://doi.org/10.5281/zenodo.6791657>).

543 The adaptive solver implementation within the GEOS-Chem atmospheric chemistry model used in this

544 work is available at <https://github.com/jimmielin/geos-chem/tree/staging/autoreducekpp> (The

545 International GEOS-Chem Community, 2022; <https://doi.org/10.5281/zenodo.6791655>).

546 **References**

- 547 Alvanos, M. & Christoudias, T. (2017). GPU-accelerated atmospheric chemical kinetics in the
548 ECHAM/MESSy (EMAC) Earth system model (version 2.52), *Geoscientific Model Development*, 10,
549 3679-3693. <https://doi.org/10.5194/gmd-10-3679-2017>
- 550 Bates, K. H. & Jacob, D. J. (2019). A new model mechanism for atmospheric oxidation of isoprene:
551 global effects on oxidants, nitrogen oxides, organic products, and secondary organic aerosol,
552 *Atmospheric Chemistry and Physics*, 19, 9613–9640. <https://doi.org/10.5194/acp-19-9613-2019>
- 553 Bates, K. H., & Jacob, D. J. (2020)., An expanded definition of the odd oxygen family for tropospheric
554 ozone budgets: implications for ozone lifetime and stratospheric influence, *Geophysical Research*
555 *Letters*, 47, e2019GL084486. <https://doi.org/10.1029/2019GL084486>
- 556 Bates, K. H., Jacob, D. J., Li, K., Ivatt, P. D., Evans, M. J., Yan, Y., & Lin, J. (2021). Development and
557 evaluation of a new compact mechanism for aromatic oxidation in atmospheric models, *Atmospheric*
558 *Chemistry and Physics*, 21, 18351–18374. <https://doi.org/10.5194/acp-21-18351-2021>
- 559 Bey, I., Jacob, D. J., Yantosca, R. M., Logan, J. A., Field, B. D., Fiore, A. M., Li, Q., Liu, H. Y., Mickley,
560 L. J., & Schultz, M. G. (2001). Global modeling of tropospheric chemistry with assimilated
561 meteorology: Model description and evaluation, *Journal of Geophysical Research: Atmospheres*, 106,
562 23073–23095. <https://doi.org/10.1029/2001JD000807>
- 563 Bian, H., & Prather, M. J. (2002). Fast-J2: Accurate Simulation of Stratospheric Photolysis in Global
564 Chemical Models, *Journal of Atmospheric Chemistry*, 41, 281-296.
565 <https://doi.org/10.1023/A:1014980619462>
- 566 Brasseur, G. P. & Jacob, D. J. (2017). *Modeling of atmospheric chemistry*, Cambridge: Cambridge
567 University Press. <https://doi.org/10.1017/9781316544754>
- 568 Brown-Steiner, B., Selin, N. E., Prinn, R., Tilmes, S., Emmons, L., Lamarque, J.-F., & Cameron-Smith,
569 P. (2018). Evaluating simplified chemical mechanisms within present-day simulations of the
570 Community Earth System Model version 1.2 with CAM4 (CESM1.2 CAM-chem): MOZART-4 vs.
571 Reduced Hydrocarbon vs. Super-Fast chemistry, *Geoscientific Model Development*, 11, 4155–4174.
572 <https://doi.org/10.5194/gmd-11-4155-2018>
- 573 Brown, P. N., Byrne, G. D., & Hindmarsh, A. C. (1989). VODE: A Variable-Coefficient ODE Solver,
574 *SIAM Journal on Scientific and Statistical Computing*, 10(5), 1038-1051.
575 <https://doi.org/10.1137/0910062>
- 576 Damian, V., Sandu, A., Damian, M., Potra, F., & Carmichael, G. R. (2002). The kinetic preprocessor
577 KPP-a software environment for solving chemical kinetics, *Computers & Chemical Engineering*,
578 26(11), 1567–1579. [https://doi.org/10.1016/S0098-1354\(02\)00128-X](https://doi.org/10.1016/S0098-1354(02)00128-X)

- 579 Dawson, M. L., Guzman, C., Curtis, J. H., Acosta, M., Zhu, S., Dabdub, D., Conley, A., West, M.,
580 Riemer, N., & Jorba, O. (2022). Chemistry Across Multiple Phases (CAMP) version 1.0: an integrated
581 multiphase chemistry model, *Geoscientific Model Development*, 15, 3663-3689.
582 <https://doi.org/10.5194/gmd-15-3663-2022>
- 583 Djouad, R., & Sportisse, B. (2002). Partitioning techniques and lumping computation for reducing
584 chemical kinetics. APLA: An automatic partitioning and lumping algorithm, *Applied Numerical*
585 *Mathematics*, 43(4), 383-398. [https://doi.org/10.1016/S0168-9274\(02\)00111-3](https://doi.org/10.1016/S0168-9274(02)00111-3)
- 586 Eastham, S. D., Long, M. S., Keller, C. A., Lundgren, E., Yantosca, R. M., Zhuang, J., Li, C., Lee, C. J.,
587 Yannetti, M., Auer, B. M., Clune, T. L., Kouatchou, J., Putman, W. M., Thompson, M. A., Trayanov, A.
588 L., Molod, A. M., Martin, R. V., & Jacob, D. J. (2018). GEOS-Chem High Performance (GCHP v11-
589 02c): a next-generation implementation of the GEOS-Chem chemical transport model for massively
590 parallel applications, *Geoscientific Model Development*, 11, 2941–2953. [https://doi.org/10.5194/gmd-](https://doi.org/10.5194/gmd-11-2941-2018)
591 [11-2941-2018](https://doi.org/10.5194/gmd-11-2941-2018)
- 592 Fast, J. D., Gustafson Jr., W. I., Easter, R. C., Zaveri, R. A., Barnard, J. C., Chapman, E. G., Grell, G. A.,
593 & Peckham, S. E. (2006). Evolution of ozone, particulates, and aerosol direct radiative forcing in the
594 vicinity of Houston using a fully coupled meteorology-chemistry-aerosol model, *Journal of Geophysical*
595 *Research: Atmospheres*, 111(D21), D21305. <https://doi.org/10.1029/2005JD006721>
- 596 Gong, W., & Cho, H.-R. (1993). A numerical scheme for the integration of the gas-phase chemical rate
597 equations in three-dimensional atmospheric models, *Atmospheric Environment. Part A. General Topics*,
598 27(14), 2147-2160. [https://doi.org/10.1016/0960-1686\(93\)90044-Y](https://doi.org/10.1016/0960-1686(93)90044-Y)
- 599 Grell, G. A., Peckham, S. E., Schmitz, R., McKeen, S. A., Frost, G., Skamarock, W. C., & Eder, B.
600 (2005). Fully coupled “online” chemistry within the WRF model, *Atmospheric Environment*, 39(37),
601 6957–6975. <https://doi.org/10.1016/j.atmosenv.2005.04.027>
- 602 Hairer, E. & Wanner, G. (1991). *Solving Ordinary Differential Equations II. Stiff and Differential-*
603 *Algebraic Problems*, Berlin: Springer.
- 604 Hakami, A., Henze, D. K., Seinfeld, J. H., Singh, K., Sandu, A., Kim, S., Byun, D., and Li, Q. (2007).
605 The Adjoint of CMAQ, *Environmental Science & Technology*, 41, 7807-7817.
606 <https://doi.org/10.1021/es070944p>
- 607 Henze, D. K., Hakami, A., & Seinfeld, J. H. (2007). Development of the adjoint of GEOS-Chem,
608 *Atmospheric Chemistry and Physics*, 7, 2413-2433. <https://doi.org/10.5194/acp-7-2413-2007>
- 609 Holmes, C. D., Bertram, T. H., Confer, K. L., Graham, K. A., Ronan, A. C., Wirks, C. K., & Shah, V.
610 (2019). The Role of Clouds in the Tropospheric NO_x cycle: A New Modeling Approach for Cloud
611 Chemistry and Its Global Implications, *Geophysical Research Letters*, 46(9), 4980-4990.
612 <https://doi.org/10.1029/2019GL081990>

- 613 Jacobson, M. Z., & Turco, R. P. (1994). SMVGEAR: A sparse-matrix, vectorized gear code for
614 atmospheric models, *Atmospheric Environment*, 28(2), 273-284. [https://doi.org/10.1016/1352-
615 2310\(94\)90102-3](https://doi.org/10.1016/1352-2310(94)90102-3)
- 616 Jacobson, M. Z. (1995). Computation of global photochemistry with SMVGEAR II, *Atmospheric
617 Environment*, 29(18), 2541–2546. [https://doi.org/10.1016/1352-2310\(95\)00194-4](https://doi.org/10.1016/1352-2310(95)00194-4)
- 618 Jöckel, P., Kerkweg, A., Pozzer, A., Sander, R., Tost, H., Riede, H., Baumgaertner, A., Gromov, S., &
619 Kern, B. (2010). Development cycle 2 of the Modular Earth Submodel System (MESSy2), *Geoscientific
620 Model Development*, 3, 717–752. <https://doi.org/10.5194/gmd-3-717-2010>
- 621 Keller, C. A., & Evans, M. J. (2019). Application of random forest regression to the calculation of gas-
622 phase chemistry within the GEOS-Chem chemistry model v10, *Geoscientific Model Development*, 12,
623 1209–1225. <https://doi.org/10.5194/gmd-12-1209-2019>
- 624 Kelp, M. M., Jacob, D. J., Kutz, J. N., Marshall, J. D., & Tessum, C. W. (2020). Toward stable, general
625 machine-learned models of the atmospheric chemical system, *Journal of Geophysical Research:
626 Atmospheres*, 125(23), e2020JD032759. <https://doi.org/10.1029/2020JD032759>
- 627 Kelp, M. M., Jacob, D. J., Lin, H., & Sulprizio, M. P. (2022). An Online-Learned Neural Network
628 Chemical Solver for Stable Long-Term Global Simulations of Atmospheric Chemistry, *Journal of
629 Advances in Modeling Earth Systems*, 14(6), e2021MS002926. <https://doi.org/10.1029/2021MS002926>
- 630 Long, M. S., & Lin, H. (2022). KineticPreProcessor/KPP-AR-boxmodel: GC_v13.4-AR-BoxModel
631 [Software], *Zenodo*. <https://doi.org/10.5281/zenodo.6791657>
- 632 Mao, J., Jacob, D. J., Evans, M. J., Olson, J. R., Ren, X., Brune, W. H., Clair, J. M. St., Crouse, J. D.,
633 Spencer, K. M., Beaver, M. R., Wennberg, P. O., Cubison, M. J., Jimenez, J. L., Fried, A., Weibring, P.,
634 Walega, J. G., Hall, S. R., Weinheimer, A. J., Cohen, R. C., Chen, G., Crawford, J. H., McNaughton, C.,
635 Clarke, A. D., Jaeglé, L., Fisher, J. A., Yantosca, R. M., Le Sager, P., & Carouge, C. (2010). Chemistry
636 of hydrogen oxide radicals (HO_x) in the Arctic troposphere in spring, *Atmospheric Chemistry and
637 Physics*, 10, 5823–5838. <https://doi.org/10.5194/acp-10-5823-2010>
- 638 Moch, J. M., Dovrou, E., Mickley, L. J., Keutsch, F. N., Liu, Z., Wang, Y., Dombek, T. L., Kuwata, M.,
639 Budisulistiorini, S. H., Yang, L., Decesari, S., Paglione, M., Alexander, B., Shao, J., Munger, J. W., &
640 Jacob, D. J. (2020). Global Importance of Hydroxymethanesulfonate in Ambient Particulate Matter:
641 Implications for Air Quality, *Journal of Geophysical Research: Atmospheres*, 125(18), e2020JD032706.
642 <https://doi.org/10.1029/2020JD032706>
- 643 Philip, S., Martin, R. V., and Keller, C. A. (2016). Sensitivity of chemistry-transport model simulations to
644 the duration of chemical and transport operators: a case study with GEOS-Chem v10-01, *Geoscientific
645 Model Development*, 9, 1683-1695. <https://doi.org/10.5194/gmd-9-1683-2016>

- 646 Rastigejev, Y., Brenner, M. P., & Jacob, D. J. (2007). Spatial Reduction Algorithm for Atmospheric
647 Chemical Transport Models, *PNAS*, 104(35), 13875-13880. <https://doi.org/10.1073/pnas.0705649104>
- 648 Rosenbrock, H. H. (1963). Some general implicit processes for the numerical solution of differential
649 equations, *The Computer Journal*, 5(4), 329-330, <https://doi.org/10.1093/comjnl/5.4.329>
- 650 Sander, R., Baumgaertner, A., Cabrera-Perez, D., Frank, F., Gromov, S., Grooß, J.-U., Harder, H.,
651 Huijnen, V., Jöckel, P., Karydis, V. A., Niemeyer, K. E., Pozzer, A., Riede, H., Schultz, M. G.,
652 Taraborrelli, D., & Tauer, S. (2019). The community atmospheric chemistry box model
653 CAABA/MECCA-4.0, *Geoscientific Model Development*, 12, 1365–1385. [https://doi.org/10.5194/gmd-](https://doi.org/10.5194/gmd-12-1365-2019)
654 [12-1365-2019](https://doi.org/10.5194/gmd-12-1365-2019)
- 655 Sandu, A., Verwer, J., Blom, J., Spee, E., Carmichael, G., & Potra, F. (1997). Benchmarking stiff ode
656 solvers for atmospheric chemistry problems II: Rosenbrock solvers, *Atmospheric Environment*, 31(20),
657 3459–3472. [https://doi.org/10.1016/S1352-2310\(97\)83212-8](https://doi.org/10.1016/S1352-2310(97)83212-8)
- 658 Sandu, A., & Sander, R. (2006). Technical note: Simulating chemical systems in Fortran90 and Matlab
659 with the Kinetic PreProcessor KPP-2.1, *Atmospheric Chemistry and Physics*, 6, 187–195.
660 <https://doi.org/10.5194/acp-6-187-2006>
- 661 Sandu, A., Sander, R., Long, M. S., Yantosca, R. M., Lin, H., Shen, L., & Jacob, D. J. (2022).
662 KineticPreProcessor/KPP: The Kinetic PreProcessor (KPP) 3.0.0 [Software], *Zenodo*.
663 <https://doi.org/10.5281/zenodo.7308373>
- 664 Santillana, M., Le Sager, P., Jacob, D. J., & Brenner, M. P. (2010). An adaptive reduction algorithm for
665 efficient chemical calculations in global atmospheric chemistry models, *Atmospheric Environment*,
666 44(35), 4426–4431. <https://doi.org/10.1016/j.atmosenv.2010.07.044>
- 667 Shen, L., Jacob, D. J., Santillana, M., Wang, X., & Chen, W. (2020). An adaptive method for speeding up
668 the numerical integration of chemical mechanisms in atmospheric chemistry models: application to
669 GEOS-Chem version 12.0.0, *Geoscientific Model Development*, 13, 2475–2486.
670 <https://doi.org/10.5194/gmd-13-2475-2020>
- 671 Shen, L., Jacob, D. J., Santillana, M., Bates, K., Zhuang, J., & Chen, W. (2022). A machine-learning-
672 guided adaptive algorithm to reduce the computational cost of integrating kinetics in global atmospheric
673 chemistry models: application to GEOS-Chem versions 12.0.0 and 12.9.1, *Geoscientific Model*
674 *Development*, 15, 1677–1687. <https://doi.org/10.5194/gmd-15-1677-2022>
- 675 The International GEOS-Chem Community. (2022). *jimmie/lin/geos-chem: AR-GC-archival_13.4*
676 [Software], *Zenodo*. <https://doi.org/10.5281/zenodo.6791655>
- 677 Wang, X., Jacob, D. J., Downs, W., Zhai, S., Zhu, L., Shah, V., Holmes, C. D., Sherwen, T., Alexander,
678 B., Evans, M. J., Eastham, S. D., Neuman, J. A., Veres, P. R., Koenig, T. K., Volkamer, R., Huey, L. G.,
679 Bannan, T. J., Percival, C. J., Lee, B. H., & Thornton, J. A. (2021). Global tropospheric halogen (Cl, Br,

680 I) chemistry and its impact on oxidants, *Atmospheric Chemistry and Physics*, 21, 13973–13996.
681 <https://doi.org/10.5194/acp-21-13973-2021>

682 Young, T. R., & Boris, J. P. (1977). A Numerical Technique for Solving Stiff Ordinary Differential
683 Equations Associated with the Chemical Kinetics of Reactive-Flow Problems, *Journal of Physical
684 Chemistry*, 81(25), 2424–2427. <https://doi.org/10.1021/j100540a018>

685 Zhao, S., Russell, M. G., Hakami, A., Capps, S. L., Turner, M. D., Henze, D. K., Percell, P. B., Resler, J.,
686 Shen, H., Russell, A. G., Nenes, A., Pappin, A. J., Napelenok, S. L., Bash, J. O., Fahey, K. M.,
687 Carmichael, G. R., Stanier, C. O., & Chai, T. (2020). A multiphase CMAQ version 5.0 adjoint,
688 *Geoscientific Model Development*, 13, 2925–2944. <https://doi.org/10.5194/gmd-13-2925-2020>

689 Zhuang, J., Jacob, D. J., Lin, H., Lundgren, E. W., Yantosca, R. M., Gaya, J. F., Sulprizio, M. P., &
690 Eastham, S. D. (2020). Enabling High-Performance Cloud Computing for Earth Science Modeling on
691 Over a Thousand Cores: Application to the GEOS-Chem Atmospheric Chemistry Model, *Journal of
692 Advances in Modeling Earth Systems*, 12(5), e2020MS002064. <https://doi.org/10.1029/2020MS002064>